Available online at www.sciencedirect.com
ScienceDirect
Journal of Molecular Catalysis B: Enzymatic 44 (2007) 20–26
JOURNAL OF MOLECULAR CATALYSIS B: ENZYMATIC
www.elsevier.com/locate/molcatb

An experimental and theoretical study of *Coprinus cinereus* peroxidase-catalyzed biodegradation of isoelectronic to dioxin recalcitrants

A. Ziemys [a,b,*], J. Kulys [a,c]

[a] *Institute of Biochemistry, Department of Enzyme Chemistry, Mokslininku 12, 08662 Vilnius, Lithuania*
[b] *Vytautas Magnus University, Vileikos 8, 44404 Kaunas, Lithuania*
[c] *Vilnius Gediminas Technical University, Faculty of Fundamental Sciences, Department of Chemistry and Bioengineering, Sauletekio Avenue 11, 10223 Vilnius, Lithuania*

Received 7 November 2005; received in revised form 20 July 2006; accepted 28 July 2006
Available online 20 September 2006

Abstract

Isoelectronic to dibenzo-*p*-dioxin (DBD) compounds (ID) containing nitrogen and/or sulfur atom instead of oxygen atom can be oxidized in the presence of fungal peroxidase. To elucidate the structure/activity relationship the redox potential of ID's was determined and correlated with calculated properties from *ab initio* calculations. The redox potential of ID's varied between 0.16 and 1.46 V versus standard calomel electrode (SCE) in acetonitrile. Spectral measurements and *ab initio* quantum chemical calculations showed that the redox potential correlated with the quantity of heteroatom conjugation with the 6π-aromatic system. The reactivity of ID's decreased if the redox potential of ID's increased. The calculations of docking and molecular dynamics revealed that all ID's may form the stable complexes in the active center of peroxidase. The acquired results permitted to conclude that low reactivity of ID's and their halogenated derivatives is associated with the high redox potential of recalcitrants.

Keywords: Biodegradation; Heme peroxidase; 2,3,7,8-Tetrachlorodibenzo-*p*-dioxin; Kinetics; Modeling

1. Introduction

Dibenzo-*p*-dioxins are group of poisonous compounds with different toxic activities: immunotoxic, embryotoxic, teratogenic, neurotoxic and carcinogenic [1–3]. Dibenzo-*p*-dioxins and other isoelectronic compounds (ID) containing sulfur and nitrogen atoms are being formed as a by-product in consumption processes, coal burning and in preparation of large quantities of man-made organic compounds. Natural degradation of these compounds is a serious environmental problem.

It was demonstrated that lignin peroxidase could oxidize dioxins by generating a high potential mediator, i.e. a cation radical of veratryl alcohol (CRV) [4]. It was hypothesized that other heme peroxidases, i.e. cap ink peroxidase (CiP) was also involved into biodegradation of xenobiotics though it did not generate CRV at a significant rate [5].

The task of this report was to study the possibility of ID's biodegradation with CiP. In order to explore biodegradability, the enzymatic activity and redox potentials of the compounds were measured and modeling techniques such as *ab initio* calculations, substrate docking into enzyme active center and molecular dynamics were performed.

2. Materials and methods

2.1. Experimental

10-Methyl phenothiazine (MP) and 10-methyl phenoxazine (MPX) were synthesized in Novo Nordisk A/S (Denmark). 5,10-Dihydro, 5-10-dimethyl phenazine (DMF; "Aldrich"), thianthrene (TA; "Aldrich"), phenoxathiin (TXA; "Aldrich"), 1-phenoxatiin carboxylic acid (TXA1) and 4,6-phenoxathiin dicarboxylic acid (TXA46) were received from Novo Nordisk

* Corresponding author at: Institute of Biochemistry, Department of Enzyme Chemistry, Mokslininku 12, 08662 Vilnius, Lithuania.
E-mail address: a3arzi@vaidila.vdu.lt (A. Ziemys).

1381-1177/$ – see front matter © 2006 Elsevier B.V. All rights reserved.
doi:10.1016/j.molcatb.2006.07.015

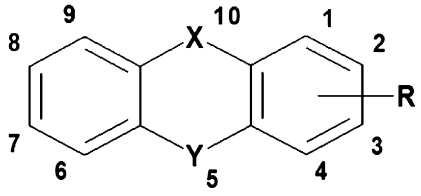

	X	Y	R
DMF	N-CH$_3$	N-CH$_3$	-H
MP	N-CH$_3$	S	-H
MPX	N-CH$_3$	O	-H
TA	S	S	-H
TXA	S	O	-H
TXA1	S	O	-COOH (1)
TXA46	S	O	-COOH (4,6)
DBD	O	O	-H
TCDD	O	O	-Cl (2,3,7,8)

Fig. 1. Structures of the investigated compounds.

A/S (Denmark). The structure of compounds is depicted in Fig. 1. Acetonitrile (HPLC grade) was a product of "Aldrich".

Recombinant fungal peroxidase from *Coprinus cinereus* as a commercial product of Novo Nordisk A/S was additionally purified by anion exchange chromatography to a Reinheit Zahl (A_{405}/A_{208}) of 2.61. The enzyme was homogeneous as assessed by SDS-PAGE. The concentration of CiP was determined spectrophotometrically at 405 nm by using the molar absorption of $1.08 \times 10^5\ M^{-1}\ cm^{-1}$ [5]. Solution of H_2O_2 was prepared from perhydrol (30%) and concentrations were established by using the molar absorption of $39.4\ M^{-1}\ cm^{-1}$ at 240 nm [6].

For the establishment of the formal reduction potential (redox potential E), cyclic voltammetry (CV) on the glassy carbon electrode was performed by using an electroanalytical system (Cypress Systems Inc., USA) and the glassy carbon electrode (model CS-1087, Cypress Systems Inc., USA). As a reference, a saturated calomel electrode (SCE saturated with KC1, model K-401, Radiometer, Denmark) and as an auxiliary electrode a Pt-wire (diameter 0.2 mm, length 4 cm) mounted on the end of the reference electrode were used. The measurements were performed in acetonitrile at room temperature. As support electrolyte 50 mM of tetraethylammonium tetrafluoroborate ("Aldrich") was used. The potential scan rate varied from 12 to 200 mV/s. The electrode potential varied in range from 0 to 2600 mV. Each CV measurement was performed on a freshly polished electrode. The formal redox potential for reversible or quasi-reversible conversion was estimated by using the relationship $E = (E_{p,a} + E_{p,c})/2$, where $E_{p,a}$ and $E_{p,c}$ were the anodic and cathodic peaks, respectively. The redox potential of TXA, TXA1 and TXA46 was estimated as $E = E_{p,a} - 50$ mV. The potential values in the text are depicted versus SCE at the scan rate of 100 mV/s. The coefficient of variation of the redox potential determination varied from 0.1 to 4.0%.

Absorption of ID's was measured with the computer-controlled Beckman DU-8B spectrophotometer in the range from 220 to 800 nm. The compounds were dissolved in redistilled methanol. Steady-state kinetics of the substrates oxidation was studied by a spectrophotometric method, too. The measurements were carried out at room temperature 25 °C in presence of 0.1 mM H_2O_2 at pH 8.5 in 50 mM Tris–HCl buffer with 2.5 % (v/v) of acetonitrile. The absorbance change was approximated by single decay with offset and the calculated initial rate (V) was used for further analysis. V of TA, TXA, TXA1 and TXA46 was proportional to substrate concentration, therefore an apparent bimolecular rate constant (k_{ox}) was stated as $V/[E][S]$ where $[E]$ and $[S]$ corresponded to the enzyme and substrate concentration, respectively. The change in the extinction coefficient during the substrate oxidation was determined by the total oxidation of the substrates in the presence of the excess of peroxidase and hydrogen peroxide.

2.2. Theory

Ab initio calculations were performed by using the Gaussian 98 W package [7]. The geometries of molecules were optimized with the HF (Hatree–Fock) theory and 6-31G* basis set. All energies are expressed in atomic units (a.u.; 1 a.u. = 27.2116 eV). The hydrophobicity of compounds was calculated with VEGA [8] and Crippen scheme of log P.

The simulations of the substrate docking were performed with AutoDock 3.0.5 [9] in the active center of *Arthromyces ramosus* peroxidase (ARP). ARP and CiP structures are almost identical [10]. The crystal data of ARP [11] were downloaded from the Protein Data Bank. All water molecules in the active center of ARP were removed with the exception of those on a distal side of heme vicinity. In order to model catalytically active state of ARP, i.e. compound I/II, the distance of Fe=O bond was set to 1.77 Å, i.e. the average Fe=O distance of compounds I and II of horseradish peroxidase [12]. Atomic interaction energy grid maps were calculated with the 0.375 Å grid spacing forming the cubic box centered on the active side of peroxidases on the heme side exposed to water. The space of the cubic box covered the active side of peroxidases and the rest protein. The electrostatic interaction energy grid used a distance-dependent dielectric function of Mehler–Solmajer [13]. The docking was accomplished using the Lamarckian genetic algorithm. The number of individuals in populations was set 100. The maximum number of generation was 27,000. The number of the top individuals that are guaranteed to survive into the next generation was 1. The probability of performing local search on an individual was set to 0.1. Each docking was assigned to make 200 runs. The Mulliken charges for dockings were estimated from calculations with the STO-3G (Slater type orbitals) basis set under geometries optimized by the HF/3-21G method. Minimum basis sets were used to calculate Mulliken charges as there is less ambiguity in indicating the center of the atomic orbital function in an atom where a charge should be assigned.

Molecular dynamics (MD) simulations for complexes of ID compounds in the active center of ARP were performed with GROMACS 3.2.1 program suit [14,15] and GROMOS-96 43a1 force field [16]. ID–ARP complexes were taken from docking calculation results. GROMOS-96 43a1 force field was modified to model active state of heme peroxidase by binding oxygen atom to Fe atom of the heme. The partial atomic

Table 1
The kinetic, spectral and redox properties of ID compounds (25 °C)

ID	λ_{max} (nm)	ε ($\times 10^{-4}$ M^{-1} cm^{-1})	E (mV) vs. SCE	K_m ($\times 10^6$ M)	k_{ox} (M^{-1} s^{-1})
DMF	245 336	5.36 0.84	164 ± 1.0	Not determined	
MP	252 307	3.00 0.35	714 ± 2.3	8.2 [20]	58×10^6 [20]
MPX	237 317	3.20 0.71	628 ± 1.2	3.0 [20]	240×10^6 [20]
TA	255	3.29	1235 ± 37	–	2.9×10^2
TXA	237 295	2.01 0.20	1193 ± 6	–	1.1×10^2
TXA1	243 300 350	1.31 0.19 0.21	1212 ± 2	–	2.0×10^2
TXA46	245 307	1.15 0.19	1462 ± 7	–	<100

charges for compound-I were calculated with HF theory and STO-3G basis set. Charges were manually adopted for charge groups in compound-I topology wit +1.4 on Fe and −0.8 on O atoms. Fe=O bond was set to 1.67 Å and bond force constant to 5.7×10^6 kJ/(mol nm^4), which was calculated from experimental IR data at 814 cm^{-1} [17]. N–Fe=O angle was set to 90° with force constant 420 kJ/mol, which was fitted from N–Fe–N data of GROMOS-96 43a1 force field. Heme topology modification adopting compound-I was tested separately to ensure compound-I energetic and structural stability.

The modeled systems were energy-minimized using the steepest descent method with no constrains. Minimized structures were supplied to 100 ps position-restrained dynamics with 2 fs integration step, where lengths of all bond in the modeled systems was constrained with LINCS algorithm. Berendsen temperature and pressure coupling scheme was used. During the position-restrained dynamics calculations the temperature was maintained close to 300 K and the pressure was 1 bar. Particle-mesh Ewald scheme was used to treat non-bonded electrostatics and twin range cut-off scheme was used for non-bonded interaction (Lennard-Jones potential; LJ) treatment. The long-range cut-off was set 1.0 and 1.0 nm for electrostatics and LJ. System atoms were supplied with velocities generated with Maxwellian distribution.

The MD simulations during 1 ns were performed on the structures obtained after position-restrained dynamics with 1 fs integration step. All modeled systems were dissolved with SPC (simple point charge) water solvent leaving 1 nm free solvent space around dissolved ID–ARP complex. Total modeled system charge was set to zero by dissolving sodium cations. The topologies for compounds were generated with PRODRG2 server [18].

3. Results

All ID compounds share similar electronic structure and are almost identical to the structure of dibenzo-*p*-dioxin (DBD) or 2,3,7,8-tetrachlorodibenzo-*p*-dioxin (TCDD). All compounds share the same conjugated structure, i.e. two 6π-electron systems of benzene rings that are conjugated by n-electron pairs of heteroatoms. The conjugation effect of the later depends on their nature and modulates overall system conjugation. The carboxylic substitutes were introduced into ID's to increase the solubility of the compounds in a buffer solution. An oxidation of ID compounds with heme peroxidase is associated directly with a single electron donation and that property directly depends on overall system conjugation. The importance of a conjugation effect for electrical conduction properties of single-molecule, which depends directly on the delocalization of the molecular electronic orbitals also, was demonstrated experimentally, recently [19]. Therefore, the investigation of ID containing oxygen, nitrogen and sulfur atoms will reflect the chemical and electronic structure peculiarities, which drive the enzymatic biodegradability of ID with the heme peroxidase via an oxidation.

Absorption of the compounds in UV region was recorded in methanol as the basis for kinetic measurements and for experimental elucidations of electronic structures. ID absorbed in the range from 230 to 350 nm. All ID have two distinct peaks: one peak at 240–250 nm and the second one at 300–336 nm (Table 1). An exception was observed for TA, which has only one peak at 255 nm, and for TXA1, which has three peaks: one peak at 243 nm and other two small peaks at 300 and 350 nm, respectively. The analysis of absorption of non-substituted ID revealed that the second absorption peak of DMF was located at the largest wavelength, whereas the absorptions of other compounds were at shorter wavelengths. The compounds fall into the following rank DMF > MPX > MP > TXA > TA. The absorption in longer wavelengths is associated with the larger conjugation of hetero atoms (O, N, S) with two 6π-aromatic systems.

Recently, some theoretical examinations of DBD and TCDD spectra were performed using complete active space SCF followed by the multireference second-order perturbative approach (CASSCF/CASPT2) [21,22]. DBD spectra calculation fitted

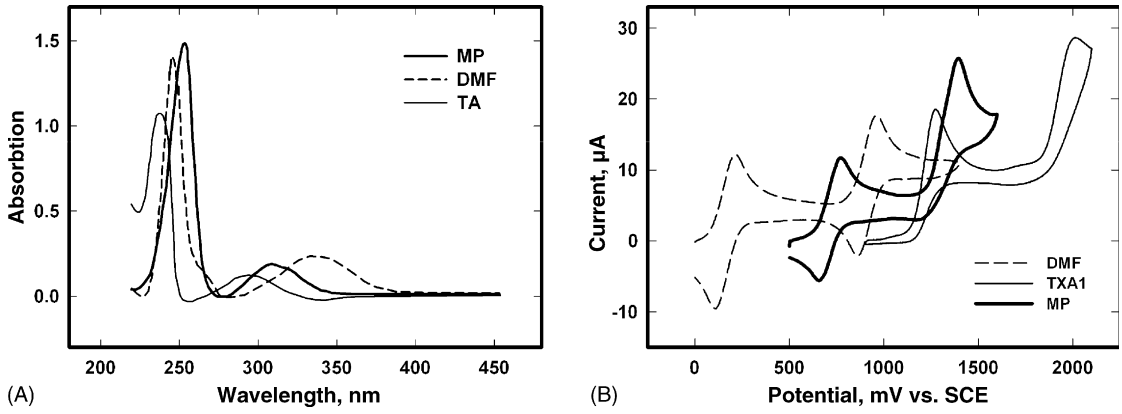

Fig. 2. The absorption spectra (A) and cyclic voltammetry (B) of DMF, MP and TXA1. Potential scan rate 100 mV/s (B).

well the experimental spectra of DBD [21] in the main absorption bands: 200–235 nm (high intensity) and 265–310 nm (broad low-intensity). Similar calculation of absorption of TCDD revealed the same two band structure at wavelengths 200–240 and 280–320 nm [22]. The main oscillation in high-intensity band of DBD and TCDD comes from π–π* transition, while low-intensity band has n–π* transition. The results of the calculations and referred experimental spectra of DBD and TCDD in [21,22] show big similarity to investigated here ID compounds and possess two basic band system separated by a region of very low absorption. DBD high-intensity band is blue-shifted comparing to ID compounds while low-intensity band is closest to the same band in the spectra of TXA. The spectra of TCDD from [22] occupied almost the same wavelengths compared to ID compounds. The present spectra comparison shows that DBD and TCDD share similar electronic structure and along with geometrical similarities their enzymatic reactivity toward enzymatic biodegradability can be rationalized further.

The fungal peroxidase CiP was used as the enzyme catalyzing the ID oxidation. The reactivity of MP and MPX has been determined before [20]. The wavelengths of 255, 237 and 243 nm were chosen for the measurement of the kinetic parameters of TA, TXA and TXA1 oxidation, respectively, since the largest absorbance change was observed at these wavelengths during oxidation. The calculated apparent bimolecular constants were $(2.9 \pm 0.3) \times 10^2\,M^{-1}\,s^{-1}$ for TA, $(1.1 \pm 0.2) \times 10^2\,M^{-1}\,s^{-1}$ for TXA and $(2.0 \pm 0.2) \times 10^2\,M^{-1}\,s^{-1}$ for TXA1 (Table 1). The comparison of these values with the results of MP and MPX oxidation showed that the oxidation rate of TXA1 was 300,000 and 1,200,000 times less (Table 1).

It is well known that an electron conjugation plays the important role in electron transfer reaction. Experimentally electron-donating properties of ID were revealed by the redox potential, which was determined electrochemically. The quasi-reversible single electron transfer was established for DMF, MP and MPX. Moreover, DMF demonstrated the quasi-reversible two-electron transfer (Fig. 2B). MP and MPX also showed quasi-reversible electron transfer, but in contrast to DMF, the two-electron transfer was irreversible.

The electrochemical conversion of TA at 1.0–1.5 V disclosed the quasi-reversible character for the single electron transfer. However, the potential scan at 1.0–2.0 V indicated that the doubly oxidized compound splits very fast. TXA, TXA1 and TXA46 demonstrated the irreversible electrochemical conversions during one- and two-electron transfer reaction. The redox potential of these compounds was larger than 1.2 V. The reason of the low stability of oxidized species is the high potential that significantly exceeds the potential of DMF, MP and MPX. The redox potential of ID changed in the range between 160 and 1445 mV (Table 1). The potential of non-substituted ID falls into the rank DMF < MPX < MP < TXA < TA, which is opposite to the absorption rank described above. This confirms the preposition about the importance of the heteroatom orbital conjugation based on the spectral measurements.

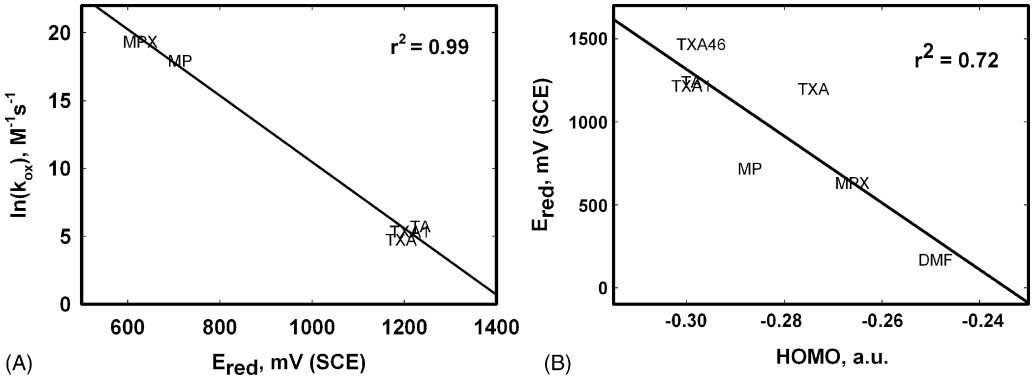

Fig. 3. Correlations of the redox potential vs. the enzymatic reactivity (A) and HOMO vs. the redox potential (B).

Table 2
Calculated properties of ID compounds

ID	HOMO (a.u.)	Docking (kcal/mol)	log *P*
DMF	−0.265	−7.3	3.4
MP	−0.292	−6.9	3.8
MPX	−0.257	−7.5	3.2
TA	−0.309	−6.5	4.2
TXA	−0.280	−7.1	3.6
TXA1	−0.303	−6.7[a]	3.2
TXA46	−0.293	−6.6[a]	2.7
DBD	−0.289	−7.2	3.1
TCDD	−0.314	−8.5	5.3

[a] Dissociated carboxylic groups.

The first step in DBD and ID oxidation is a single electron reduction of compound I of peroxidase [4]. The kinetic analysis of MPX, MP, TXA1 and TXA46 compounds oxidation showed that the enzymatic reactivity is closely related to electron donating properties of ID and that was determined by the redox measurements (Table 1). The investigation of all ID compounds by the redox and spectral absorption measurements proved that heteroatom conjugation into the common electronic system determinates electron-donating property. The biodegradations or oxidation of ID can be analyzed in the framework of the Marcus outer-sphere electron-transfer theory [21], where a free energy of reaction, reorganization energy of molecules and overlap of molecular orbitals of donor and acceptor guide an electron transfer. The correlation of the reactivity with the redox potential showed good linear dependence ($r^2 = 0.99$) (Fig. 3A). Since electrons are withdrawn from highest occupied molecular orbitals (HOMO) during an electron transfer from the substrates to compound-I of CiP, the HOMO energy of substrates determines the redox potential. *Ab initio* calculations under RHF/6-31G* theory were performed to calculate energies of HOMO. According to *ab initio* calculations, the structures of DBD, TCDD and TXA are totally planar. The rest compounds are not planar due to the steric effects introduced by substitutes in rings. TA structure was found to be very bended through S–S axis and has V-shape. Among the investigated ID compounds, HOMO with the lowest energy was calculated for TA and TXA1 (Table 2). The difference between HOMO of DMF, MPX and TXA1, TA was about 0.04 a.u., i.e., about 1.1 eV. Since the TA structure was significantly bent along the S–S axis, both benzene rings have the minimum conjugation effect and HOMO energy is very low. Based on HOMO energy values ID compounds fall into the rank MPX > DMF > TXA > MP > TA that is very similar to the rank of absorptions.

According to HOMO values and the correlation versus experimental results the best electron donors should be DMF and MPX (Table 2). Calculations revealed that DBD and MP have similar HOMO energies at −0.29 a.u. Calculated HOMO energy for TCDD have the lowest value from all investigated compounds −0.31 a.u. and is similar to TXA1 and TA. While TCDD and TXA1 are planar structures, TA structure is bended along S–S axis. Low HOMO values for TCDD and TXA1 can be explained by effects of substitutes, but low HOMO energy of TA can be related to a low conjugation. The calculated lowest values can

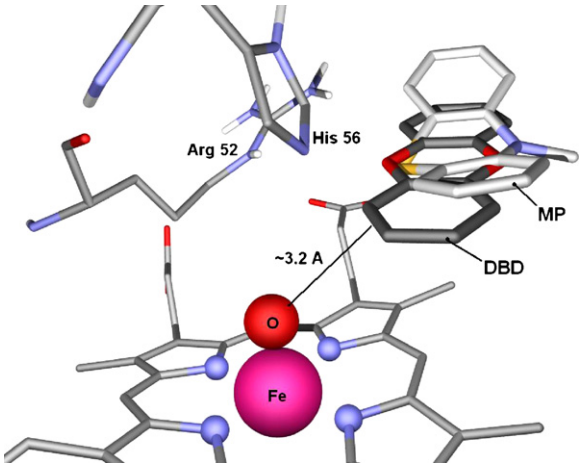

Fig. 4. Docking of DBD and MP in the compound I of ARP.

be supported by measured redox potential, which was found for TXA1 and TA highest between ID compounds along with TXA46. The ionization potentials of TA and TCDD are 7.90 eV [24] and 7.99 eV [25]. The comparison of ionization potentials of TA and TCDD reveals the similar values also. Those values of ionization potentials are largest compared to MPX, TXA and DBD, which are 7.15 eV [26], 7.72 eV [27] and 7.598 eV [25], respectively. The comparison of HOMO, redox potential and available ionization potential values reveal that TA and TCDD has lowest electron donating properties, which is important elucidating the ability to degrade TCDD with enzymatic oxidation. However, the ionization potential and HOMO values of DBD show that the electron donating properties should be comparable to MP, which possesses significant enzymatic reactivity toward CiP.

HOMO energy correlations to E_{red} and k_{ox} revealed significant dependences with $r^2 = 0.72$ and 0.73 (Fig. 3B), respectively.

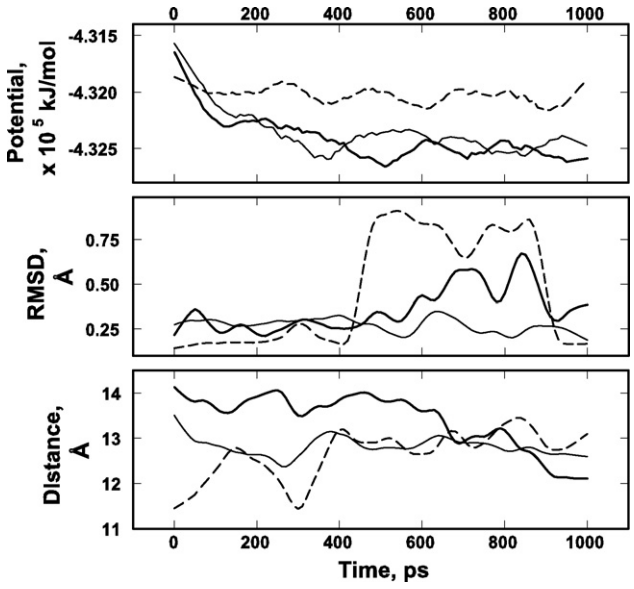

Fig. 5. Energetic and structural behavior of substrate–protein complexes (DBD, tiny; MP, bold; TCDD, dashed). From top: potential energy of a system, RMSD of a ligand, distance between centers of masses of a ligand and an enzyme.

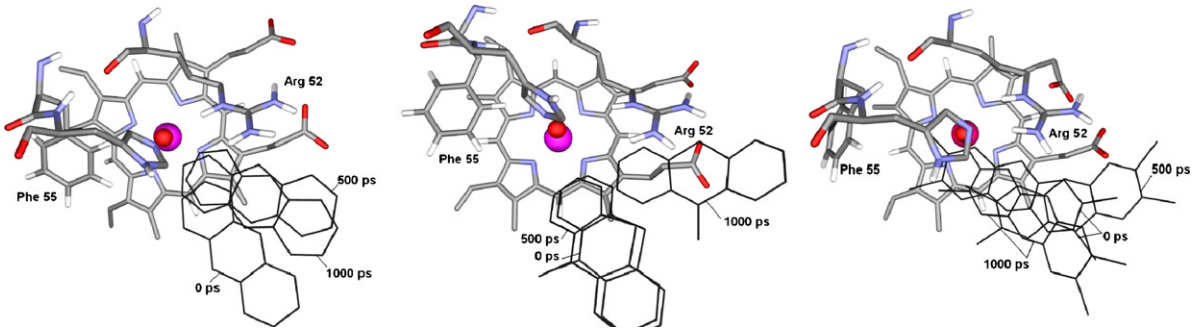

Fig. 6. Snapshots of substrate–ARP complex dynamics after 0, 0.5 and 1 ns (from left: DBD, MP, TCDD).

According to HOMO versus k_{ox} correlations, the crude estimations of k_{ox} values for DBD and TCDD would be 1.2×10^6 and $1.3 \times 10^3\ M^{-1}\ s^{-1}$. Predicted reactivity of DBD and its tetrachlorinated analog is different almost 1000 times. However, predicted reactivity of TCDD is very small and even less than measured reactivity of TXA46.

To accomplish a single electron reaction transfer reaction, the substrates should combine in the active center. Docking and MD calculations were applied to explore the enzyme–substrate complex formation and its stability. Docking calculations revealed that investigated substrates dock at the active center of ARP with different affinities and the energies vary from −6.5 kcal/mol (TA) to −8.5 kcal/mol (TCDD). Although TA and TCDD are the most hydrophobic compounds from log *P* calculations (Table 2), their affinity to the active center is opposite. The low affinity of TA is determined by bended structure, which makes steric hindrances. Comparing TCDD to the rest compounds it is clear that hydrophobicity plays significant role in high affinity for TCDD. Nonchlorinated DBD possess similar log *P* to other compounds, including the most enzymatically reactive. It docks similar to MP in the active center of ARP (Fig. 4).

Stability of enzyme–substrate complex in solvent was explored by MD simulations for 1 ns of time period with compounds MPX, DBD and TCDD. Potential energy profile of the whole system with MP and DBD showed dropping potential energy during the first 400 ps and systems stayed stable during the rest time (Fig. 5). In case of TCDD the relative stability of potential energy during all simulation was calculated with slightly decrease of the energy. However, the structural analysis revealed more dynamic behavior of the substrates. Root mean square deviation (RMSD) and distances between mass center of protein and ligand were calculated. The stable trajectory dynamics of RMSD was determined for DBD, but the rest two compounds undergo structural rearrangements. The largest rearrangements were calculated for TCDD, although both TCDD and MP have RMSD disturbances in the period 500–900 ps (Fig. 5). Despite the detected structural rearrangements of substrates in the active center of ARP, these compound stay in there, because the RMSD values are not large and all calculated distance between mass centers of protein and ligand converge to similar values from 11–14 to 12–13 Å (Fig. 5). These results show that substrate–ARP complexes share the similar geometry or donor–acceptor distance is almost identical between different complexes. After MD simulations all substrates were found in the active center of ARP with different variations from starting points (Fig. 6).

4. Conclusions

The analysis of overall results show that the electron transfer in the enzyme active center is predominantly chemically controlled and the reactivity of ID with CiP is determined by a free energy of the reaction [23]. The correlation $\ln(k_{ox})$ with the redox potential showed a very good agreement within the experimental results. The correlations of HOMO with $\ln(k_{ox})$ and E_{red} have led to good correlation with r^2 around 0.7. Good correlations mean that the electron transfer rate for MPX, MP, TXA1 and TCDD is almost determined by the free energy of the reaction, as it was mentioned above. The docking and MD calculations indicate that substrates are bonded at distances not larger than 4 Å from electron accepting centre. At this distance, the electron exchange rate is fast; electrons can tunnel over distances up to 17 Å at the rate of $720\ s^{-1}$ that was measured for the fastest determined (MPX) reaction [20]. On the basis of described, performed crude estimations of the reactivity of DBD and TCDD with CiP reveal that DBD could be biodegraded with efficiency comparable to MP. However, the degradability of compound TCDD is almost impossible due to low HOMO and, possibly, high redox potential. Rejecting the solubility problem of TCDD in water or water-based buffers, large hydrophobicity could possibly induce non-productive complex of TCDD–ARP in the cavity of the active center of ARP.

The biodegradability of DBD and ID recalcitrants along with TCDD is related to redox properties cumulative with the hydrophobicity or solubility problem. The most appropriate way of biodegradation of halogenated high-redox ID compounds like TCDD is dehalogenation step to drop redox potential and make better solubility in water prior to the oxidation with heme peroxidases.

Acknowledgements

This research was supported by Lithuanian State Science and Studies Foundation, project no. C-03048. We thank Palle Schneider (Novo Nordisk A/S, Denmark) for providing enzyme and substrates, Irina Bratkovskaja for the kinetics of low reactive ID's oxidation recording.

References

[1] M. Sharp, J. Environ. Monit. 2 (2000) 89.
[2] S.A. Skene, I.C. Dewhurst, M. Greenberg, Hum. Toxicol. 8 (3) (1989) 173.
[3] M.A. Fingerhut, W.E. Halperin, D.A. Marlow, L.A. Piacitelli, P.A. Honchar, M.H. Sweeney, A.L. Greife, P.A. Dill, K. Steenl, A.J. Suruda, New Engl. J. Med. 324 (4) (1991) 212.
[4] O.K. Joshi, M.H. Gold, Biochemistry 33 (1994) 10969.
[5] M.B. Andersen, Y. Hsuanyu, K.G. Welinder, P. Schneider, H.B. Dunford, Acta Chim. Scand. 45 (1991) 1080.
[6] D. Nelson, L.A. Kiesow, Anal. Biochem. 49 (1972) 474.
[7] M.J. Frisch, G.W. Trucks, H.B. Schlegel, et al., Gaussian 98, Revision A.9, Gaussian Inc., Pittsburgh, PA, 1995–1998.
[8] A. Pedretti, L. Villa, G. Vistoli, J. Comp. Aided Mol. Design 18 (2004) 167.
[9] D.S. Goodsell, A.J. Olson, Proteins: Struct. Funct. Gen. 8 (1990) 195.
[10] K. Tsukamoto, H. Itakura, K. Sato, K. Fukuyama, S. Miura, S. Takahashi, H. Ikezawa, T. Hosoya, Biochemistry 38 (1999) 12558.
[11] N. Kunishima, K. Fukuyama, H. Matsubara, H. Hatanaka, Y. Shibano, T. Amachi, J. Mol. Biol. 235 (1994) 331.
[12] G.I. Berglund, G.H. Carlsson, A.T. Smith, H. Szoke, A. Henriksen, J. Hajdu, Nature 417 (6887) (2002) 463.
[13] E.L. Mehler, T. Solmajer, Protein Eng. 4 (1991) 903.
[14] H.J.C. Berendsen, D. van der Spoel, R. van Drunen, Comp. Phys. Commun. 91 (1995) 43.
[15] E. Lindahl, B. Hess, D. van der Spoel, J. Mol. Mod. 7 (2001) 306.
[16] W.F. van Gunsteren, S.R. Billeter, A.A. Eising, P.H. Hunenberger, P. Kruger, A.E. Mark, W.R.P. Scott, I.G. Tironi, Biomolecular Simulation: The GROMOS96 Manual and User Guide, Hochschulverlag AG an der ETH Zurich, Zurich, Switzerland, 1996.
[17] H. Fujii, Coord. Chem. Rev. 226 (2002) 51.
[18] A.W. Schuettelkopf, D.M.F. van Aalten, Acta Crystallogr. D 60 (2004) 1355.
[19] T. Dadosh, Y. Gordin, R. Krahne, I. Khivrich, D. Mahalu, V. Frydman, J. Sperling, A. Yacoby, I. Bar-Joseph, Nature 436 (7051) (2005) 677.
[20] J. Kulys, K. Krikstopaitis, A. Ziemys, J. Biol. Inorg. Chem. 5 (2000) 333.
[21] I. Ljubic, A. Sabljic, J. Phys. Chem. A 109 (2005) 8209.
[22] I. Ljubic, A. Sabljic, J. Phys. Chem. A 110 (110) (2006) 4524.
[23] R.A. Marcus, N. Sutin, Biochim. Biophys. Acta 811 (1985) 265.
[24] B.K. Park, W.K. Lee, Bull. Korean Chem. Soc. 24 (5) (2003) 655.
[25] T. Uchimura, Anal. Sci. 21 (2005) 395.
[26] L.N. Domelsmith, L.L. Munchausen, K.N. Houk, J. Am. Chem. Soc. 99 (20) (1977) 6506.
[27] M.E. Amato, A. Grassi, K.J. Irgolic, G.C. Pappalardo, L. Radics, Organometallics 12 (1993) 775.